

The Complex Nature of Turbulence Transition in Boundary Layer Flow Over a Flat Surface

JC Chen* and Chen Weijia

School of Civil and Environmental Engineering

Block N1 Nanyang Avenue, Nanyang Technological University, Singapore 639798

*E-mail: JimChen@ntu.edu.sg

ABSTRACT

This is a review of the literature on turbulence transition in free stream boundary layer flows. The transition to turbulence is induced by the classical method of introducing an external perturbation into the flow in the form of a vibrating ribbon. Three defining aspects of the subsequent transition phenomenon are considered: its physics, mathematics, and numerical simulation. The physics describes the physical nature of turbulence with depiction of the generation and interaction of disturbance waves and the formation of turbulent flow structures. The mathematics converts the physical problem into its governing equations and boundary conditions. The numerical simulation then solves the governing equations to realize the flow behavior. An example simulation of two dimensional boundary layer flow in the linear instability stage demonstrates wave amplification and damping dynamics.

1. INTRODUCTION

I direct your attention to Figures 1a and 1b. It illustrates the phenomenon of turbulence transition in boundary layer flow over a flat surface and the stages of development leading to the eventual turbulence. Turbulence transition is the process whereby a laminar flow field evolves to become turbulent, signaled by the presence of random oscillations in the flow velocities and generation of small-scale vortices. To fully understand turbulence transition demands thoughtful and interconnected consideration of three elements that describe its nature: its physics, mathematics, and numerical simulation. They are interdependent, mutually illuminating elements that form a problem of sprawling complexity. They also examine the problem from a spectrum of perspectives. First, a far-sighted perspective is needed that views the overall problem in its macroscopic, general terms, such as its experimental settings, governing equations, and boundary conditions. Accompanying it is a precision-oriented, detail-solicitous view of the minute, microscopic flow intricacies, such as small-scale turbulence vortices and infinitesimal instability wave interactions that transpire in the flow. The capacity and tolerance to switch between varying degrees of these orthogonally-oriented perspectives is necessary to systematically break down this problem. This study demonstrates a deconstruction of the phenomenon of turbulence transition in order to gain an appreciation of its very complex nature.

For the element of physics, the overarching objective is to gain knowledge of the physical nature of transition to turbulence. Turbulence transition in boundary layer flow manifests over a multi-stage progression, as illustrated in the classical experiment of Schubauer and Skramstad, 1947 shown in Figure 1a [2]. In this experiment, external perturbations are introduced at the flow entrance using a vibrating ribbon at the bottom wall. The perturbations generate waves that propagate downstream. Figure 1b shows that the generated waves first enter into a region of linear interactions with one another where they amplify or damp in accordance with the relationship between the phases of their propagation [1]. By linear interaction, in the governing equations that describe the wave propagation, the Navier-Stokes (NS) equations, the linear terms will dominate the non-linear terms. As the waves travel further downstream, the non-linear terms in the governing NS equations will become activated and increase in their relative significance to the linear terms. These non-linear interactions will generate additional waves into the flow. The location of this development is the region labeled “non-linear region” in Figure 1b [1, 3–9]. In the non-linear region, the newly generated waves will continue to interact non-linearly and spin off additional vortices that are acutely sensitive and increasingly unstable to the presence of external disturbances. The vortices will reach a point where they are unsustainable

(a)

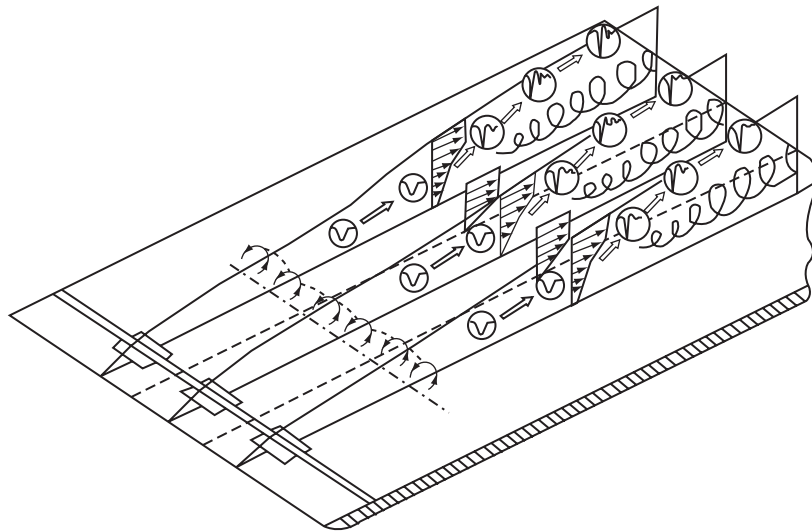


Figure 1a. Schematic of the classical experimental setup for turbulence transition in boundary layer flow. A vibrating ribbon is placed at the base of the flow entrance to introduce perturbations into the flow. Reprinted from Kachanov, 1994 [1] with permission from Annual Reviews.

(b)

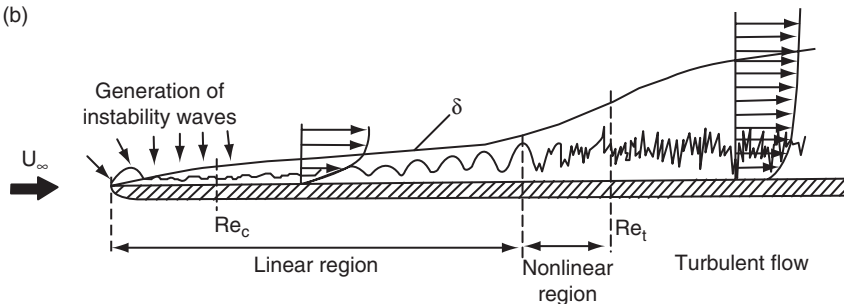


Figure 1b. Stages of development in turbulence transition. Reprinted from Kachanov, 1994 [1] with permission from Annual Reviews.

and breakdown to form random oscillations that define flow turbulence in the turbulent flow region of Figure 1b [1, 4, 7–10]. This problem, turbulence transition, is the focus of extensive research. It traces its roots to the classical field of turbulent fluid dynamics, one of the long-standing unsolved mysteries of science. Just like the general field of turbulence fluid dynamics from which it branches, the transition to turbulence is a problem of notorious, multitudinous complexity. Considering the physics of the problem is to deconstruct its physical architecture comprising flow structures and wave interactions that emerge along the pathway towards turbulence.

For the element of mathematics, the physical problem of turbulence transition is cast into its corresponding set of mathematical governing equations in order to generate solutions of the flow behavior. The governing equations for turbulence transition in boundary layer flows are the NS equations with appropriate boundary conditions [11, 12]. The fact that the NS equations are the correct governing equations stands without dispute. However, the selection of the appropriate accompanying boundary conditions is a topic of much debate [13]. When defining the proper boundary conditions, two fundamental principles are pivotal. One is that the boundary conditions together with the NS equations should render the set of equations to be well-posed, that is, the set of equations can, in fact, be solved to generate a unique solution [12]. Second, the solution should be physically accurate in that it does, in fact, depict the behavior of the flow under the given conditions. Meeting both criteria, in essence, is an exercise in proper definition of the problem in its mathematical terms. This is no trivial issue, and much controversy surrounds it.

The NS equations have other forms that can be used for greater ease in defining the problem and achieving an accurate solution. A popular alternative strategy is to convert the original NS equations from its primitive form to the Vorticity Transport Equation [12, 14, 15]. However, this exercise creates a new problem in that questions now arise as to whether the converted Vorticity Transport Equation is, in fact, equivalent to its original NS equation antecedent [16]. The answer to this question lies in the correct definition of the boundary conditions for the Vorticity Transport Equation. The equivalence between the Vorticity Transport Equation and the original NS equations is also a non-trivial topic of concern [12, 13, 16].

For the element of numerical simulation, the mathematically well-posed set of governing equations and boundary conditions must be solved numerically to realize simulations of the flow behavior [15, 17–26]. The numerical method must be capable of converging to a unique final solution. This final solution should, in turn, be an accurate depiction of the actual flow behavior. In addition, other important considerations should be included. As the transition to turbulence due to wave amplification occurs only under certain ranges of flow conditions, the numerical method must be stable across a vast range of flow parameters such as the Reynolds number, in order to encompass the specific range of interest [27]. Furthermore, the turbulent flow structures generated during transition will, in general, be microscopic in size. So, the numerical simulation should be performed at very precise levels of resolutions in order to fully visualize these microscopic structures [10]. The combination of high Reynolds number conditions where turbulence occurs and the high resolution needed to realize the turbulent structures exerts an exponentially increasing computational demand on the numerical method, with the number of required grid points scaling as $Re^{9/4}$ [28]. Therefore, a computationally efficient numerical method is necessary. In sum, the numerical method for solving the governing set of equations should be convergent to a solution that is an accurate depiction of the flow behavior, capable of resolving the microscopic turbulent flow structures, and computationally efficient. Included in this study is an example of the simulation of two-dimensional boundary layer flow in the linear instability stage of transition. The numerical method solves the Vorticity Transport Equation using a finite difference method with line iteration along the computational domain.

I direct your attention again to Figures 1a and 1b. The physical problem under investigation is boundary layer flow transition to turbulence. This problem can be cast mathematically in the form of the Vorticity Transport Equation with the appropriate boundary conditions. The mathematical governing equations are solved by a proper numerical method. The results of the numerical simulations will shed light on the nature of wave propagation and interactions that lead to the generation of turbulence. The objectives of the authors are to systematically break down and study the mosaic of complexities that comprise this problem and to invite the wider academic community into an appreciation of the complex nature of turbulence transition in boundary layer flows over a flat surface.

Section 2 presents a review of the physical phenomena comprising transition to turbulence. Section 3 discusses the conversion of the physical problem into mathematical representation of governing equations and boundary conditions. Challenges involved in deriving a well-posed set of governing equation and correct boundary conditions are considered. Section 4 then presents an example of numerical simulation of two-dimensional boundary layer flow in the linear instability stage. The numerical method solves the Vorticity Transport Equation with appropriate boundary conditions. Results of the simulation depict disturbance wave amplification and damping dynamics that are in agreement with linear stability theory.

2. PHYSICAL PHENOMENA IN TURBULENCE TRANSITION

The first element of the problem is the physical mechanisms leading to turbulence transition in boundary layer flow. A difficulty in understanding the physics of the problem is that turbulence transition is a multi-path, multi-stage phenomenon. There is more than one pathway for laminar boundary layer flow to become turbulent. Each of these paths involves multiple stages of turbulence development. Moreover, the late stages of turbulence transition involve non-linear interactions among microscopic flow structures and small-amplitude waves. Investigating the intricacies of such interactions requires rigorously fine resolutions of experimental visualizations or numerical realizations that are not practically attainable at the present time [1, 3, 29]. So, the late stages of transition where turbulence ultimately manifests remains ambiguous and mysterious. The early-stage flow and wave interaction dynamics are much better understood.

In general, the pathways to turbulence induced by perturbations at the flow entrance (Figures 1a and 1b) can be broadly categorized into two main categories. The first broad category entails transition that occurs through the generation and propagation of waves derived from an initial external disturbance of small amplitude. As the generated waves propagate downstream, they interact with one another to amplify their amplitudes, spin off secondary waves, interact with those secondary waves, and then eventually break down into turbulence. This pathway is viewed as the more traditional route in transition with wide-ranging practical applications of interest and will be referred here as normal transition [1]. On the other hand, if the amplitude of the initial disturbance is sufficiently high, then the pathway can bypass the progression of steps of wave interactions and immediately enter into breakdown into turbulence. This pathway is termed bypass transition [1]. The traditional normal transition pathway of wave interaction and amplification by small-amplitude disturbance at the entrance is the subject of focus for this review. The stages of development towards turbulence for this pathway will be reviewed here.

2.1. Receptivity

Receptivity is the name of the first stage in turbulence transition [30]. An external disturbance is introduced at the flow entrance (Figure 1a). Under suitable flow conditions such as sufficient Reynolds number, the boundary layer of the flow will become receptive to the perturbations and generate instability waves known as the Tollmien-Schlichting (TS) waves (see Figure 1b). The TS waves propagate downstream and interact to amplify or damp and can eventually lead to turbulence [1, 30]. A study of receptivity in zero pressure gradient boundary layer flow is given in Sengupta, et al., 2009 [30].

2.2. Linear Instability

The TS waves interact with one another as they propagate downstream. For sufficiently low amplitudes of external disturbances ($< 0.05\%$ of the mean flow velocity) and low Reynolds number ($< 10^4$), the interactions of the waves can be accurately described by linear stability theory [18]. Linear stability theory begins by taking the NS equations to govern the mechanisms of wave transport and then imposes two major assumptions: linearity and parallelism [1]. By linearity, the non-linear terms in the NS equations are considered to be negligible and only linear interactions are included. By parallelism, the flow field is considered to be purely parallel in the streamwise direction such that the components of the velocity in the lateral and transverse directions are neglected. Much debate has arisen regarding the validity of these assumptions, especially parallelism [1, 19]. Experimental studies have demonstrated that linear stability theory can, in fact, accurately describe the early stages of wave interactions during transition. The most famous of these studies is the classical experimental work of Schubauer and Skramstad, 1947 [2].

At the early linear instability stage of transition, the TS waves generated by the external perturbation will be two-dimensional. With the assumption of linearity and parallelism, the governing NS equation for the wave transport behavior is transformed into the classical Orr-Sommerfeld (OS) equation [25, 31, 32]:

$$\frac{i}{\alpha Re}(\phi^{IV} - 2\alpha^2\phi'' + \alpha^4\phi) + (U - c)(\phi'' - \alpha^2\phi) - U''\phi = 0. \quad (1)$$

Equation (1) depicts an eigenvalue problem with complex eigenvalue c and eigenfunction ϕ . The parameter α is the wave number of the external disturbance, c is the wave velocity of the external disturbance which is also the eigenvalue of eqn (1), Re is the Reynolds number, U is the streamwise component of the flow velocity, i is the imaginary number $\sqrt{-1}$, and the superscripts on ϕ represent orders of differentiation. For the problem of free stream boundary layer flow shown in Figures 1a and 1b, the boundary conditions for eqn (1) are [25, 31, 32]:

$$\phi(0) = \phi'(0) = 0 \quad \text{at } y = 0 \quad (\text{at the wall}) \quad (2a)$$

$$\lim_{y \rightarrow \infty} \phi(y) - \lim_{y \rightarrow \infty} \phi'(y) = 0 \quad (\text{at the free stream}). \quad (2b)$$

The stream function $\psi(x, y, t)$ of the propagating instability wave downstream can be derived from the eigenfunction of eqn (1) as [25, 31, 32]:

$$\psi(x, y, t) = \phi(y)e^{-i\alpha(x-ct)} \quad (3)$$

where x is the downstream location, y is the transverse location, and t is time. The components of the velocity of the instability wave u (streamwise velocity) and v (transverse velocity) can be directly computed from differentiating the stream function $\psi(x, y, t)$.

The OS equation has been extensively studied and numerous solution methods have been presented. Notable selections include the Compound Matrix Method by Ng and Reid, 1980 [31], the Method of Order Reduction by Van Stijn and Van de Vooren, 1980 [32], and a Chebyshev Polynomial Expansion Method by Orszag, 1971 [33].

In eqn (1), if the wave number α of the external perturbation is purely a real number, the wave will have a constant amplitude in time at a given downstream x direction [32]. The amplitude will increase with time if c_i , the imaginary part of the complex eigenvalue c , is greater than 0. The amplitude will decrease with time if $c_i < 0$ [32]. The wave only evolves temporally in this situation. On the other hand, if the frequency of the external perturbation $\omega = \alpha c$ is purely a real number, the amplitude of the wave will be constant in time but evolve spatially, increasing for $c_i > 0$, decreasing for $c_i < 0$ [32]. The flow conditions where $c_i = 0$ then delineates a point of transition known as the neutral stability curve [25, 31, 32]. The neutral stability curve distinguishes between flow conditions that are stable versus unstable to the external perturbation. Stable conditions will cause the instability waves to damp. Unstable conditions will cause the waves to amplify. An example of a neutral stability curve will be given in Figure 7.

2.3. Weakly Non-Linear and Secondary Instability

As the TS waves continue to propagate downstream, their amplification and interaction will cause additional secondary waves to be generated that are three-dimensional in nature. At this point, the flow enters into a weakly non-linear stage of transition where non-linear terms in the NS equations begin to take effect [1, 3]. The weakly non-linear interactions between the waves create a secondary instability that is susceptible to subsequent rapid amplification, randomization, and breakdown into turbulence.

Numerous models have been presented for describing the weakly non-linear stage of transition. A peculiarity regarding this stage of transition is that the pathway towards turbulence from this stage branches into a multitude of possibilities. The secondary waves that are generated from the original fundamental waves can take on a plethora of characteristics such as frequency and wave number. Further, the wave interactions can now arise from a multitude of combinations of fundamental and secondary waves. Various studies have espoused their interpretations of wave interactions occurring at this stage [1, 3, 8, 34, 35]. However, an underlying caveat that is worthy of note is that the pathway between secondary instability and turbulence is truly non-unique, and so differing views may not be mutually exclusive.

One general group of weakly non-linear models casts the wave interactions to be non-resonating and comprising one fundamental TS wave and two oblique waves. Examples of non-resonating wave models are given in Benney and Lin, 1960 [35] and Herbert, 1988 [3]. Another group of weakly non-linear models considers the wave interactions to be resonating. A classic example of this type of wave interaction is the Craik's resonant triad of one fundamental TS wave and two oblique subharmonic waves with frequency one half of the fundamental wave [8, 9]. Examples of subharmonic resonating models are given in Craik, 1971 [8] and Herbert, 1988 [3].

A classical mathematical representation of weakly non-linear wave interactions is by use of a Floquet system of differential equations [3]. In Floquet analysis, the governing equations for wave transport are again the NS equations. The disturbance is considered to be sufficiently small such that the NS equations can be linearized by eliminating the non-linear terms. The flow is also assumed to be locally parallel. The total flow u_T consists of a base flow velocity u_B and a disturbance flow velocity u_D [3]:

$$u_T = u_B + u_D. \quad (4)$$

The base flow now comprises the mean flow velocity in the boundary layer u_M , as well as, the fundamental TS wave velocity [3]:

$$u_B = u_M + Au_{TS}. \quad (5)$$

where A is the amplitude of the TS wave u_{TS} . The amplitude A is assumed to be locally constant in that it changes much more slowly than the disturbance wave oscillations. When $A = 0$, the governing equations revert back to the OS equation given in eqn (1). With these conditions, the governing equations become a Floquet system of differential equations. A solution method for the Floquet system is given in Herbert, 1988 [3]. The theoretical results of the Floquet analysis for the growth rate of waves in the downstream direction compare agreeably with experimental data showing that this method is indeed a valid representation of weakly non-linear wave interactions [3].

2.4. Non-Linear Breakdown and Flow Randomization

As the waves propagate further downstream, non-linear and non-parallel effects will become more prominent. Weakly non-linear models of wave interactions will begin to break down. The flow now enters into the fully non-linear breakdown stage that will ultimately result in randomization of the flow into turbulence. Pathways between the non-linear breakdown stage and flow randomization are again non-unique [10, 29, 36, 37]. Furthermore, the significant non-linear effects now require the use of the full NS equations with all non-linear terms included. A classical fact is that the full NS equations have no analytical solution to the present day, unlike linear and weakly non-linear stability theories. Hence, numerical simulations should be performed to obtain visualizations of the late stages of turbulence development. However, the wave interactions at the non-linear stages occur at microscopic length and time scales that call for numerical simulations with very precise levels of resolution [28]. Due to limited computational capacity of present day computers, definitive high-resolution numerical realizations of late stage non-linear breakdown and flow randomization remains a frontier in turbulent fluid dynamics research [28]. Likewise, experimental visualizations of late-stage turbulence development is also hampered by foibles in attaining spatially and temporally high-resolution images [1, 9, 38]. Thus, the mechanisms and processes that govern non-linear breakdown and flow randomization are shrouded in mystery to the present time. Some common flow patterns have been generally observed across a variety of studies. These salient commonalities form signature pieces of the mosaic that describes late-stage turbulence development. Accurate amalgamation of these pieces to reach an overall depiction of non-linear breakdown and flow randomization is a topic of continuing study. The common flow structures and patterns that have been observed at the late stages will be outlined here.

2.4.1. Spanwise Modulation of Velocity

A signature feature of the non-linear breakdown stage is that the velocity profile of the flow will become modulated in the spanwise direction [1, 3]. The flow velocities will exhibit a continuous oscillation between peaks and valleys as shown in Figure 2 [1]. The peak velocities are the locations for non-linear wave amplifications leading to flow breakdown.

2.4.2. Primary Soliton-Like Coherent Structures (SCS)

Another common feature of non-linear wave interactions is the formation of Soliton-like Coherent Structures (SCS) [1, 10, 29]. An SCS is a strong, concentrated, self-enforcing non-linear wave. It can persist for long durations of time, and it is strong in that it emerges from interactions with other SCSs with little change to its structures except for a shift in phase [1, 10, 29]. Further, non-linear interactions among the SCSs will cause the formation of a very well-known and commonly observed structure in turbulence development, the Λ -vortex [1, 10, 29].

The SCSs travel downstream at much slower speeds than the mean boundary layer flow. However, the transverse flow velocity in the SCS is close to the mean flow velocity [29]. So, the SCS will tend to shed a secondary closed vortex in the upward direction. The secondary closed vortex will interact with the Λ -vortex to form counter-rotating streamwise vortices [29]. Further, the difference in velocities between the SCSs and the mean flow will generate a high-shear layer flowing above the SCSs. The interactions among the SCSs will ultimately lead to them merging together to form elongated low-speed streaks of coherent structures along the wall of the boundary layer [29].

The SCS, Λ -vortex, secondary closed vortex, counter-rotating streamwise vortex, high-shear layer, and low-speed streak are all prominent entities in the non-linear breakdown stage [1, 10, 29]. Their interactions eventually lead to flow randomization and turbulence. Figure 3 shows the relations among some of these structures [29].

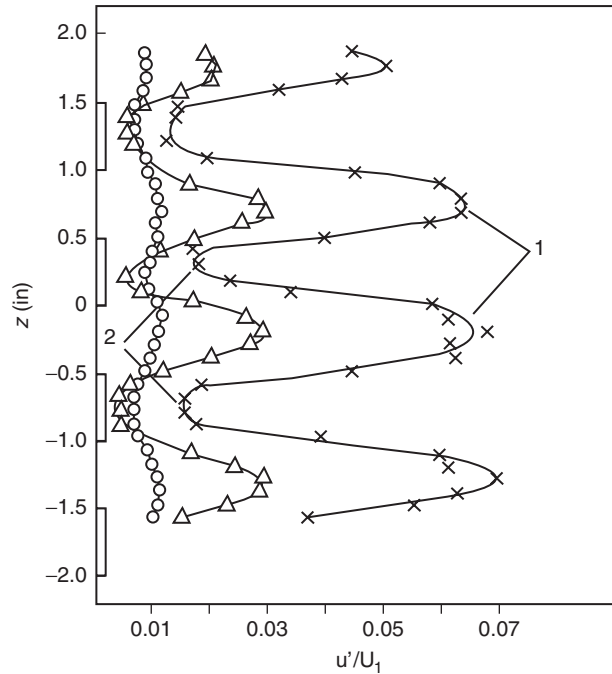


Figure 2. Spanwise modulation of peaks and valleys in flow velocities. View is from above the flow channel. Reprinted from Kachanov, 1994 [1] with permission from Annual Reviews and Cambridge University Press.

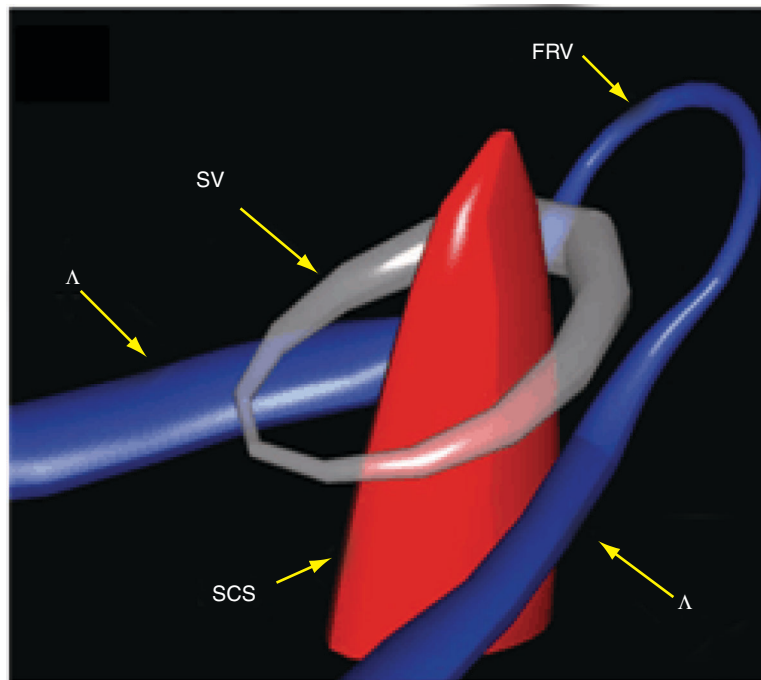


Figure 3. Interplay amongst the flow structures: Soliton-like Coherent Structure (SCS), Λ -vortex, secondary closed vortex (SV), and the first ringed vortex (FRV) also known as the Ω -vortex. Reprinted from Lee and Wu, 2008 [29] with permission from ASME.

2.4.3. Λ -Vortex

At the spanwise peak locations of flow velocities, the SCSs will induce the formation of Λ -shaped vortices [1, 10, 29]. The Λ -vortices are typically observed to be aligned along the spanwise direction or staggered. Examples of Λ -vortices are given in Figure 4. As the Λ -vortex travels downstream, its tip will lift off away from the boundary layer wall. Because the regions away from the wall will have greater streamwise velocity, the lift-off of the Λ -vortex and its interactions with the secondary closed vortex will then cause the tip of the Λ -vortex to roll up to form a hairpin-structured vortex known as the Ω -vortex (see Figure 4b) [1, 10, 29].

2.4.4. Ω -Vortex

The Ω -vortex will continue to stretch until it finally breaks away from its parent Λ -vortex. The ends of the Ω -vortex will re-connect to form a ring-shaped vortex [1, 10, 29]. The ring-shaped vortex will subsequently break up into a series of smaller ring-shaped vortices. The series of ring vortices appear as concentrated regions of high flow velocity and have been observed in both numerical simulations and experimental visualizations (see Figure 5). Because of the lifting up of the Λ -vortex at the point of formation of the Ω -vortex, the series of ring-shaped vortices will be located at the high-shear layer a small distance away from the wall [1, 10, 29]. So, the ring-shaped vortices will travel downstream at speeds faster than the Λ -vortex. This allows them to overtake and interact with other vortices downstream.

2.4.5. High Shear Layer

Slow moving structures in the boundary layer such as the SCS and the low-speed streaks causes a differentiation of velocities in the flow profile. A region of high velocity will form above the slower moving structures. This region is known as the high shear layer [1, 10, 29]. The presence of the high

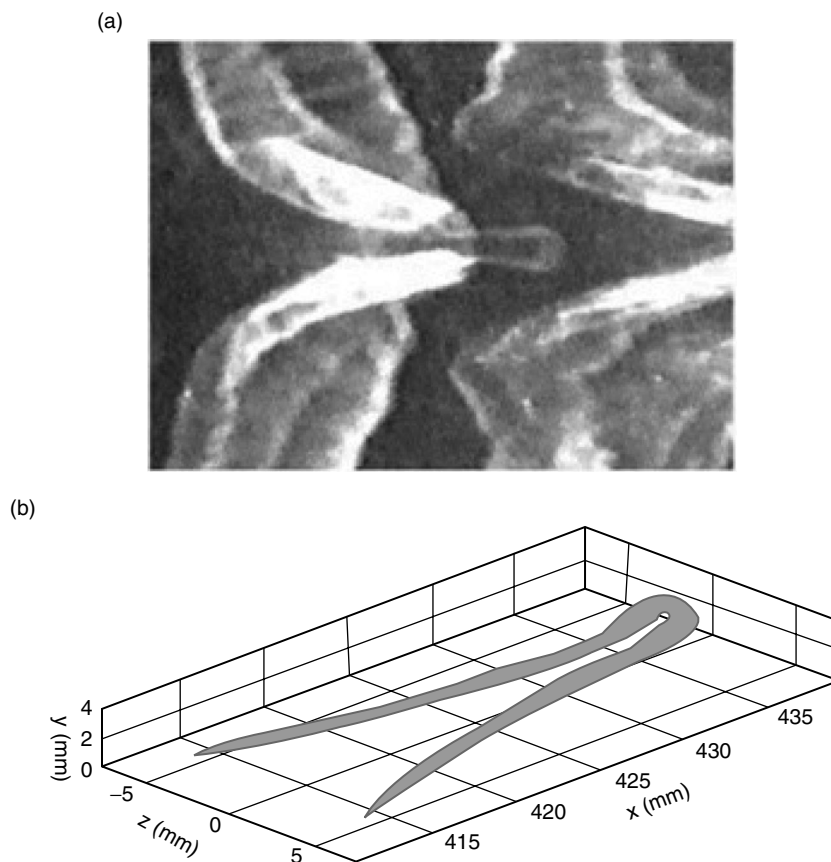


Figure 4. (a) Experimental visualization of Λ - and Ω -vortices. (b) Numerical visualization of Λ - and Ω -vortex formations. Reprinted from Borodulin, et al., 2002 [10] with permission from Springer-Verlag.

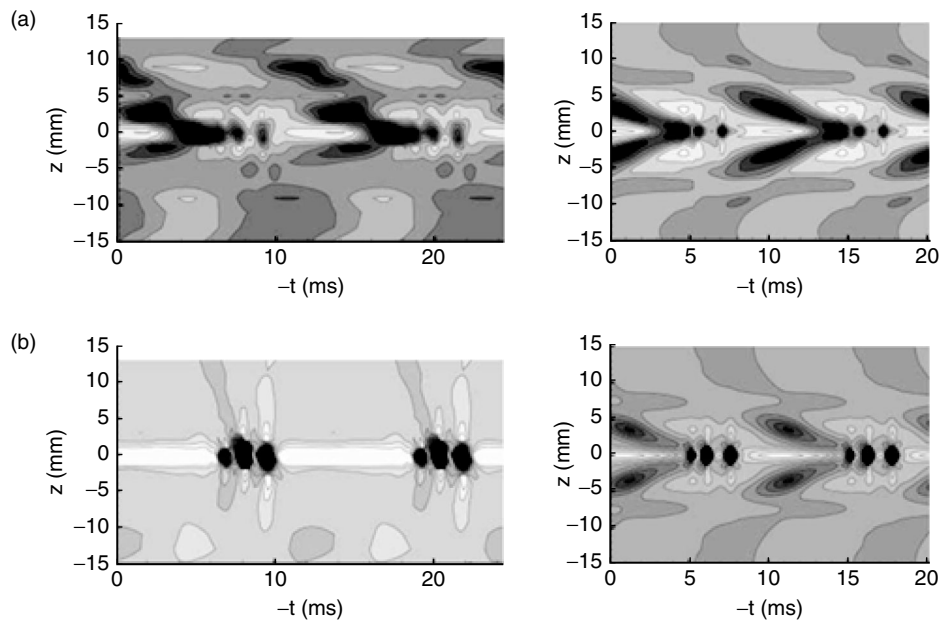


Figure 5. Contours of streamwise perturbation velocity u showing three concentrated regions of high velocity (dark regions) from the break-up of the Ω -vortex. View is from above the flow channel. Figures on the left are experimental visualizations and on the right are numerical simulations. (a) Integral of the streamwise disturbance velocity u_D in the direction normal to the wall. (b) Streamwise disturbance velocity u_D at a fixed point from the wall. Reprinted from Borodulin, et al., 2002 [10] with permission from Springer-Verlag.

shear layer produces an inflection point in the streamwise velocity profile with a distinct region of concentrated high velocity [1]. The high shear layer also acts as a conduit that channels structures such as the secondary closed vortex and the ring-shaped vortex to bypass the slower moving structures and proceed downstream.

2.4.6. Breakdown

The cacophony of the aforementioned flow structures act in concert to generate flow breakdown and randomization. The pathway to breakdown is also non-unique, and two classical pathways have been observed, the K- and N-type breakdowns.

2.4.6.1. K-Type Breakdown

K-type breakdown occurs when the amplitude of the fundamental disturbance wave is sufficiently high, generally above 1% of the mean flow [1, 9, 37]. In this case, as the fundamental wave propagates downstream, it will spin off higher-order harmonic waves with frequencies and wave numbers of $(n\omega_0, \pm\alpha\beta_0)$ where n and α are integers 1, 2, 3, ..., ω_0 , is the frequency of the fundamental wave, and β is the spanwise wave number of the fundamental wave [1, 37]. A theory describing the K-type wave interactions is the Wave Resonant (WR) concept of Kachanov and Levchenko, 1984 [1, 4]. The WR concept depicts K-type breakdown as a series of parametric, self-feeding interactions between waves of progressively higher orders, $n = 1, 2, 3, \dots$ [1, 4].

Interactions between the fundamental wave and the high-order harmonics will result in the chain of events and formations described in Sections 2.4.1 to 2.4.5 including the spanwise modulation with peaks and valleys in the velocity profile, SCS, Λ -vortex, Ω -vortex, etc. [1, 9, 37]. The Λ -vortices in K-type breakdown have been observed to be aligned along the spanwise direction [1, 9, 37]. At this point, the disturbance waves will amplify in an explosive fashion, creating temporal and spatial spikes in the flow velocity at the peak locations of the spanwise modulation [1, 9, 37]. The spikes are sudden and intermittent surges in the flow velocity. The spikes will continue to rapidly amplify until finally breaking down into turbulence. The K-type breakdown has been observed experimentally in the classical work of Klebanoff, et al., 1962 [9]. In fact, in K-type breakdown, the K stands for Klebanoff.

2.4.6.2. N-Type Breakdown

When the amplitude of the fundamental disturbance wave is not sufficient to cause the explosive K-type breakdown, flow randomization can still occur through another pathway known as the N-type breakdown [1, 4]. In N-type breakdown, the fundamental wave spins off subharmonic waves of frequencies $n\omega_0/2$ [1, 4]. The subharmonic resonant interactions among these waves lead to exponentially increasing amplification of the wave amplitudes. Thereafter, the sequence of events leading to flow randomization in N-type breakdown is similar to that of K-type [1]. Experimental observations of N-type breakdown have been presented in Kachanov and Levchenko, 1984 [4].

3. MATHEMATICALLY WELL-POSED REPRESENTATION OF THE PROBLEM

The physical problem description given in Section 2 would then need to be translated into its mathematical representation. The mathematical governing equations for incompressible flows in general are the NS equations [12, 13]:

$$\frac{\partial \vec{u}}{\partial t} + \vec{u} \cdot \nabla \vec{u} = -\nabla p + \frac{1}{Re} \nabla^2 \vec{u} \quad (6)$$

along with the continuity condition:

$$\nabla \cdot \vec{u} = 0. \quad (7)$$

This set of governing equations is complemented with the appropriate set of boundary conditions for a given flow system. For the problem of turbulence transition in boundary layer flow as shown in Figures 1a and 1b, boundary conditions need to be specified for the inflow, outflow, bottom wall, and the free stream top surface.

An alternative form of the NS equations can be obtained by taking the curl of eqn (6) to derive the Vorticity Transport Equation [12, 13, 15, 16, 21, 30, 39–41]:

$$\frac{\partial \vec{\omega}}{\partial t} + \vec{u} \cdot \nabla \vec{\omega} = \vec{\omega} \cdot \nabla \vec{u} + \frac{1}{Re} \nabla^2 \vec{\omega} \quad (8)$$

Equation (8) is complemented by the definition of the vorticity, given as [15, 21]:

$$\vec{\omega} = \nabla \times \vec{u} \quad (9)$$

and the continuity condition of eqn (7). The set of governing equation is then completed by the proper selection of boundary conditions. One boundary condition that is needed is [12, 16, 41]:

$$u = u_\Gamma \text{ on } \Gamma \quad (10)$$

where Γ is the boundary. Whether a boundary condition should be defined for the vorticity ω is an issue that remains under debate [13].

Much extensive study has been undertaken in regards to methods of solution for the set of governing equations, eqns (7 – 9) with numerous solution methods presented [12, 13, 15, 16, 21, 39–41]. One popular method is to first solve for the vorticity ω from eqn (8). Then, the velocity field u is solved from eqns (7) and (9) with ω known [12, 13, 42]. The set of equations:

$$\nabla \cdot \vec{u} = 0 \quad (11a)$$

$$\nabla \times u = \omega \quad (11b)$$

form a combination of a divergence and a curl that is known as the Cauchy-Riemann class of equations or the Div-Curl set of equations [13, 40, 41, 43]. In the Cauchy-Riemann equation type, the divergence and curl of a given vector, in this case those of u , are known. The objective is to recover the original vector u . The Cauchy-Riemann equation type describes various physical systems including electromagnetism

and fluid dynamics. In order for eqns (11a) and (11b) to be well-posed such that a unique solution can be obtained, additional constraints need to be specified as [12, 16]:

$$\int_{\Gamma} u \cdot n \, dS = 0 \tag{12a}$$

$$\nabla \cdot \bar{\omega} = 0. \tag{12b}$$

where \bar{n} is the normal vector and S is the boundary surface.

Extensive study has also been undertaken in regards to solutions of the Cauchy-Riemann Div-Curl system of equations with numerous possibilities for reaching a solution [13, 40, 41, 43]. One possible solution method is to combine the relation:

$$\Delta u = \nabla(\nabla \cdot u) - \nabla \times (\nabla \times u) \tag{13}$$

along with eqns (11a) and (11b) to derive the Poisson's Equation for the velocity [12, 13, 16, 18–20]:

$$\Delta u = -\nabla \times \omega. \tag{14}$$

Equation (14) replaces eqns (11a) and (11b) and is then combined with eqn (8) to form the governing equations along with the proper boundary conditions. By doing so, the mathematical representation is converted to the classical problem of solving the Vorticity Transport Equation followed by the Cauchy-Riemann system of equations via the Poisson's Equation [12, 13, 16, 18–20].

With this formulation, one problem is exchanged for another. First, eqn (14) is one order higher than eqns (11a) and (11b). So, an additional boundary condition needs now be defined [12]. Second, because eqn (14) is derived by differentiating eqns (11a) and (11b), the continuity condition and definition of vorticity are no longer strictly upheld. Equations (11a) and (11b) are now only upheld up to an arbitrary harmonic function [12, 16]. Ideally then, to resolve both issues, the additional boundary condition that is needed should be defined such that the continuity condition and definition of vorticity, eqns (11a) and (11b), are upheld throughout the domain. Daube, 1992 [16], Wu, et al., 1995 [41], and Rempfer, 2006 [12] provide copious discussions regarding the proper selection of the additional boundary condition.

If the additional boundary condition is defined such that the continuity condition and definition of vorticity are enforced at the boundary, then continuity and the definition of vorticity would be automatically upheld throughout the entire domain. The mathematical proof of this conclusion is given in Daube, 1992 [16]. According to the Maximal Principle, the maximum value of $|\nabla \cdot \bar{u}|$ will occur at the boundary. So, if $\nabla \cdot \bar{u} = 0$ at the boundary, it must also be so throughout the domain [12, 16]. Furthermore, as originally the definition of vorticity is only satisfied up to an arbitrary harmonic constant, stipulating $\nabla \times u = \omega$ at the boundary will select out the particular solution that forces the arbitrary harmonic function to be zero [12, 16]. So then, the full set of mathematical governing equations and boundary conditions would be given as [12, 13, 16, 18–20]:

$$\frac{\partial \bar{\omega}}{\partial t} + \bar{u} \cdot \nabla \bar{\omega} = \bar{\omega} \cdot \nabla \bar{u} + \frac{1}{Re} \nabla^2 \bar{\omega} \tag{15a}$$

$$\Delta \bar{u} = -\nabla \times \bar{\omega} \tag{15b}$$

along with boundary conditions:

$$u = u_{\Gamma} \text{ on } \Gamma \tag{16a}$$

$$\nabla \cdot u = 0 \text{ on } \Gamma \tag{16b}$$

$$\nabla \times u = \omega \text{ on } \Gamma. \tag{16c}$$

4. EXAMPLE NUMERICAL SIMULATION FOR TWO-DIMENSIONAL FLOW

4.1. Computational Domain and Governing Equations

An example of numerical simulation of two-dimensional boundary layer flow is presented here to demonstrate the physical phenomenon of disturbance wave amplification and damping in the linear instability stage. The computational discretization of the two-dimensional flow domain is shown in Figure 6. The inlet flow enters through boundary AD. The perturbation introduced to the flow by the vibrating ribbon is modeled by a frequency-driven blowing and suction velocity between x positions X_1 and X_2 . The computational domain begins after a leading distance of X_0 . Due to limitations in present computational capacity, simulations of flow domains of realistic physical dimensions as those encountered in experimental systems are impractical because of their onerous computational demand. Instead, the computational domain must be truncated at the free stream boundary CD and the outflow boundary BC in order to keep the computational time to within practical limits. The truncated boundaries then would require artificial boundary conditions that are not representations of a true physical free stream and outflow but of the conditions at the chosen point of truncation [13, 18, 19]. The artificial boundary conditions will be discussed further in Section 4.2.

With considerations for the mathematical issues discussed in Section 3, the governing equations selected in this study to investigate two-dimensional boundary layer turbulence transition flow is the Vorticity Transport Equation and its Poisson's Equations [18–20, 44]:

$$\frac{\partial \omega}{\partial t} + u \frac{\partial \omega}{\partial x} + v \frac{\partial \omega}{\partial y} = \frac{1}{Re} \frac{\partial^2 \omega}{\partial x^2} + \frac{\partial^2 \omega}{\partial y^2} \tag{17a}$$

$$\frac{1}{Re} \frac{\partial^2 u}{\partial x^2} + \frac{\partial^2 u}{\partial y^2} = \frac{\partial \omega}{\partial y} \tag{17b}$$

$$\frac{1}{Re} \frac{\partial^2 v}{\partial x^2} + \frac{\partial^2 v}{\partial y^2} = -\frac{\partial \omega}{\partial x} \tag{17c}$$

As mentioned in Section 3, eqns (17a – 17c) by themselves are not adequate to ensure the additional necessary conditions of continuity and definition of vorticity [18–20, 44]:

$$\frac{\partial u}{\partial x} + \frac{\partial v}{\partial y} = 0 \tag{18a}$$

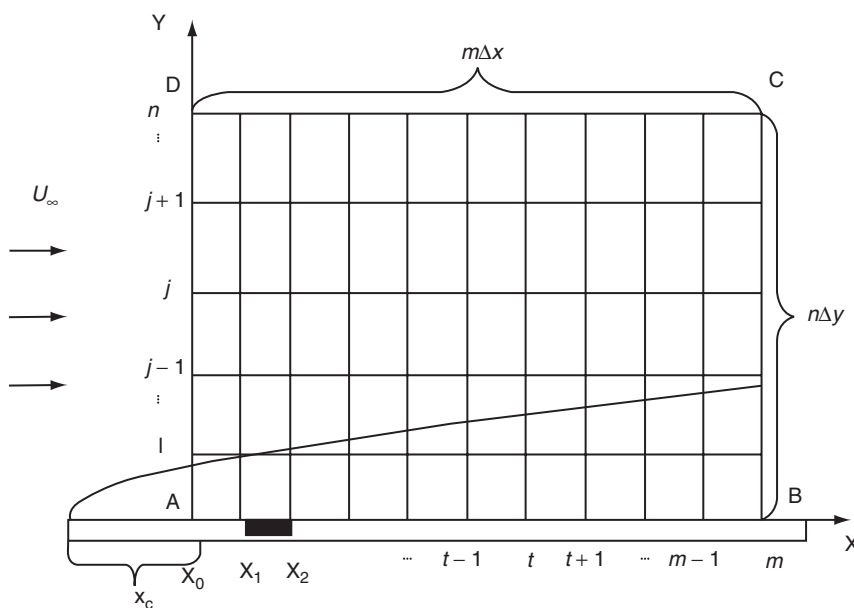


Figure 6. Discretization of computational domain.

$$\omega = \frac{\partial u}{\partial y} - \frac{1}{Re} \frac{\partial v}{\partial x}. \tag{18b}$$

These conditions need to be enforced on the boundaries through the boundary conditions. If eqns (18a) and (18b) are upheld at the boundaries, then by the Maximal Principle, they would also hold throughout the inner domain [16, 41]. The Reynolds number scaling in eqn (18b) is used to stretch the y-coordinate and the transverse velocity v .

The solution procedure for eqns (17a – 17c) requires solving first for the steady-state solution with no disturbance introduced to the flow. The steady-state solution is then used as the initial condition for the transient problem with an external disturbance added at the wall strip indicated in Figure 6. After the disturbance has been added, the total flow velocity and vorticity would then comprise the undisturbed base flow and a disturbance flow component [18–20, 44]:

$$u(x, y, t) = U(x, y) + u'(x, y, t) \tag{19a}$$

$$v(x, y, t) = V(x, y) + v'(x, y, t) \tag{19b}$$

$$\omega(x, y, t) = \Omega(x, y) + \omega'(x, y, t) \tag{19c}$$

where u, v , and vorticity ω are the total flow, U, V , and Ω are the undisturbed base flow, and $u', v',$ and ω' are the disturbance flows.

4.2. Boundary Conditions

Proper selection of the boundary conditions to accompany the governing eqns (17a – 17c) remains a hotly debated topic in the field of numerical simulations of turbulent fluid dynamics [12, 13, 16, 39, 42]. Among the complicating factors is the use of artificial boundary conditions at the free stream and outflow due to the truncation. Multiple forms of the free stream and outflow boundary conditions have been proposed and argued [13]. Also, in order to ensure the continuity condition and definition of vorticity, these conditions are additionally enforced at the boundaries. These additional conditions arise not due to the physical situation at the boundary, such as a free stream or a wall, but rather, they are implemented at the boundary solely for mathematical reasons so that the problem is well-posed with a valid, unique solution to the governing equations. Implementing the additional boundary conditions compels the solution to converge to the physically valid fields of velocity and vorticity.

The inflow boundary condition is the Blasius profile. At the bottom wall, the boundary conditions impose a no-slip velocity. At one region of the wall between locations X_1 and X_2 of Figure 6, an external perturbation is introduced into the flow by a frequency-driven blowing and suction velocity. The continuity condition and definition of vorticity are included as additional boundary conditions at the wall. Boundary conditions for the free stream and outflow boundaries are adopted from Fasel, 1980 [44]. Other related works by Fasel include Fasel, 1976 [18], Fasel and Konzelmann, 1990 [19], and Fasel, et al., 1990 [20].

4.3. Numerical Algorithm

So then, the problem is to solve the governing eqns (17a – 17c) for the computational domain shown in Figure 6. The objective is to investigate wave interactions in two-dimensional boundary layer flow to understand the linear instability stage. The numerical algorithm is adopted from Fasel, 1980 [44]. Other related works by Fasel include Fasel, 1976 [18], Fasel and Konzelmann, 1990 [19], and Fasel, et al., 1990 [20].

Immediately, another difficulty arises in this endeavor, and that is, the governing equations contain non-linear coupling of the variables u, v , and ω [18–20]. The non-linear terms $u \frac{\partial \omega}{\partial x}$ and $v \frac{\partial \omega}{\partial y}$ render the Vorticity Transport Equation difficult to solve numerically, leading to common trouble spots of numerical instability and non-convergence. So, one method to circumvent the inherent non-linearity of the governing equations is to devise a linearized solution approach. This would entail an iterative procedure where the variables u and v are first held as constants with values from the previous step in this inner sub-iteration and then solving the linearized Vorticity Transport Equation for ω . Next, the

values for u and v can be updated by solving the Poisson's Equations while holding ω constant. The inner sub-iteration loop proceeds until the values of u , v , and ω converge.

However, the decoupling demands a trade-off as it leads to poor convergence or non-convergence of the numerical method [18–20]. So, a compromise method is selected where v and ω are first solved together using u from the previous step in the inner sub-iteration, and then u is solved next to update it. A line iteration procedure is adopted where the set of variables u , v , and ω are solved one line at a time within the domain [18–20].

4.4. Results

The numerical algorithm described in Section 4.3 is validated by testing its agreement with linear stability theory. To do so, wave propagation and interaction in the linear stability region as shown in Figure 1b are investigated. In this region, wave interactions will follow the pattern of amplification and damping as mapped out by the neutral stability curve, for example Figure 7.

The validation tests are adopted from Fasel, 1980 [44]. Other related works by Fasel include Fasel, 1976 [18], Fasel and Konzelmann, 1990 [19], and Fasel, et al., 1990 [20].

Test cases are conducted to examine the behavior of the waves as they traverse downstream. In the neutral stability curve, the frequency and Reynolds numbers are scaled to their corresponding non-dimensionalized counterparts in the numerical model according to:

$$\omega_{\delta_1} = 1.72\beta\sqrt{\frac{x}{Re}} \quad (20a)$$

$$Re_{\delta_1} = 1.72\sqrt{Rex} \quad (20b)$$

where x is the downstream distance, and β is the frequency of the external disturbance.

Two test cases are investigated with simulation parameters given in Table 1. As the waves propagate downstream, they will traverse through the neutral stability curve as shown in Figure 7. The neutral stability curve predicts that the waves for Test Case 1 will amplify and those for Test Case 2 will damp.

The spatial propagation profile of the waves for Test Cases 1 and 2 at four time instances are given in Figure 8. According to the neutral stability curve of Figure 7, the waves of Test Case 1 will amplify in the downstream direction, whereas, those of Test Case 2 will damp. Examination of the wave

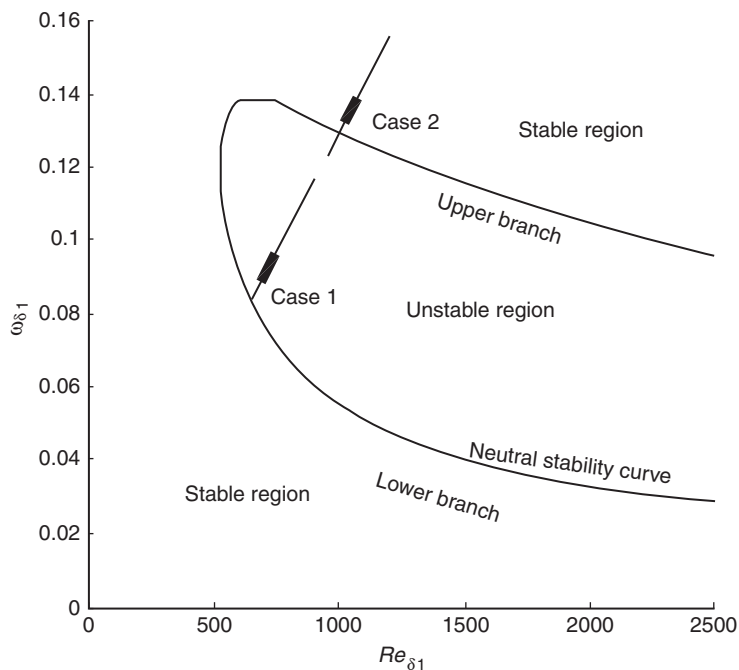


Figure 7. Traverse through the neutral stability curve for waves propagating in Test Cases 1 and 2. The location of the blowing/suction strip is indicated by the bold region.

Table 1. Simulation parameters for Test Cases 1 and 2

| | x_0 | Re_{δ_1} | m | n | Δx | Δy | Δt | β |
|-------------|-------|-----------------|-----|-----|------------|------------|------------|---------|
| Test Case 1 | 1.40 | 644 | 80 | 48 | 0.018 | 0.35 | 0.010 | 13.0 |
| Test Case 2 | 3.04 | 948 | 80 | 48 | 0.018 | 0.43 | 0.010 | 13.0 |

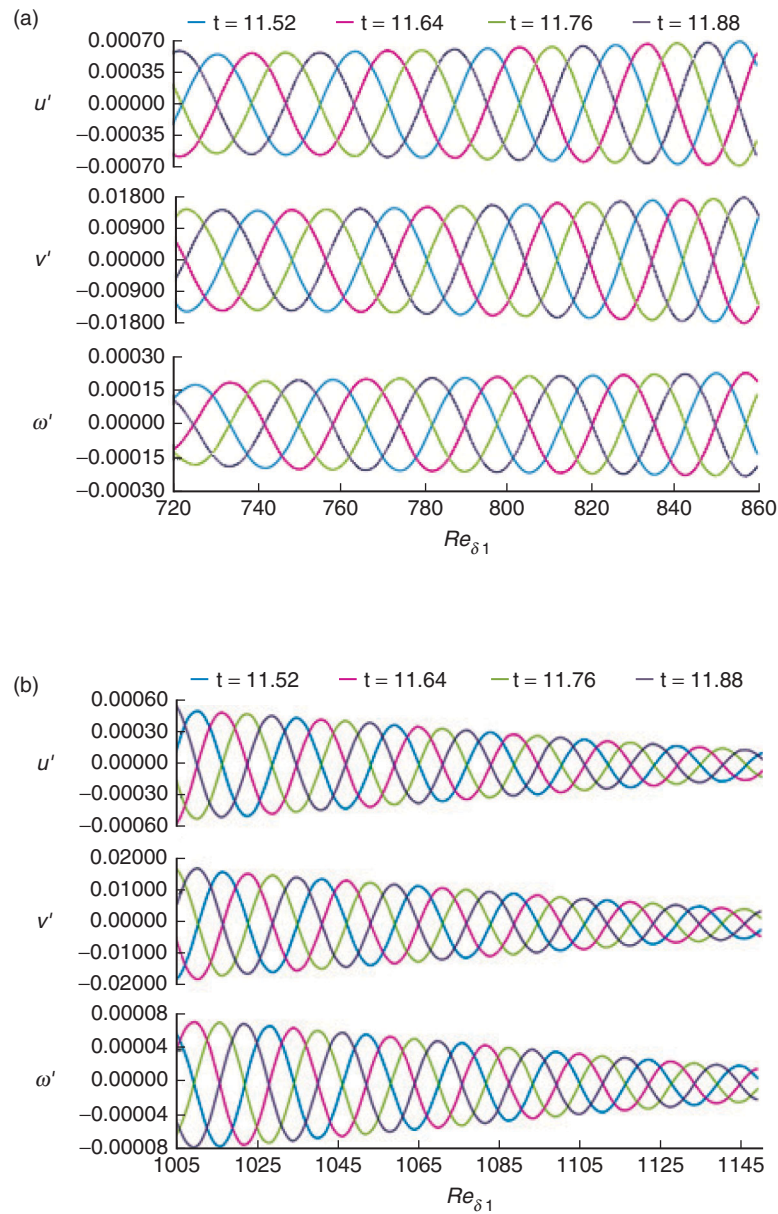


Figure 8. Wave amplification and damping in the downstream direction at four different time levels and $y/\Delta y = 3$: (a) Test Case 1 and (b) Test Case 2.

propagation patterns in Figure 8 does indeed indicate that the amplification of Test Case 1 is subtly detectable, and the damping of Test Case 2 is visually evident.

To further validate the amplification and damping of waves according to the neutral stability curve, test cases are run for complete traverses through the neutral stability curve covering both stable and unstable regions as shown in Figure 9. The simulation parameters are given in Table 2. The results of traverses at four times are given in Figure 10 and clearly show the successive

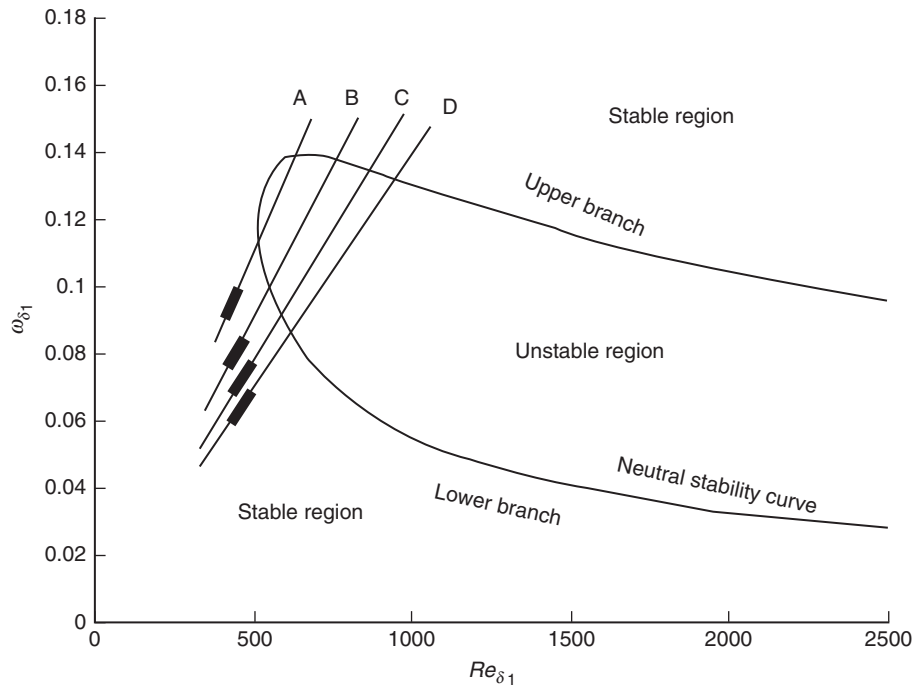


Figure 9. Test Cases A, B, C and D for complete traverse through the neutral stability curve.

Table 2. Simulation parameters for Test Cases A, B, C, and D

| | x_0 | Re_{δ_1} | m | n | Δx | Δy | Δt | β |
|--------|-------|-----------------|-----|-----|------------|------------|------------|---------|
| Case A | 0.48 | 376 | 220 | 110 | 0.005 | 0.12 | 0.007 | 22.0 |
| Case B | 0.40 | 344 | 235 | 110 | 0.008 | 0.14 | 0.008 | 18.0 |
| Case C | 0.37 | 330 | 226 | 110 | 0.012 | 0.15 | 0.008 | 15.7 |
| Case D | 0.38 | 335 | 220 | 110 | 0.015 | 0.16 | 0.010 | 14.0 |

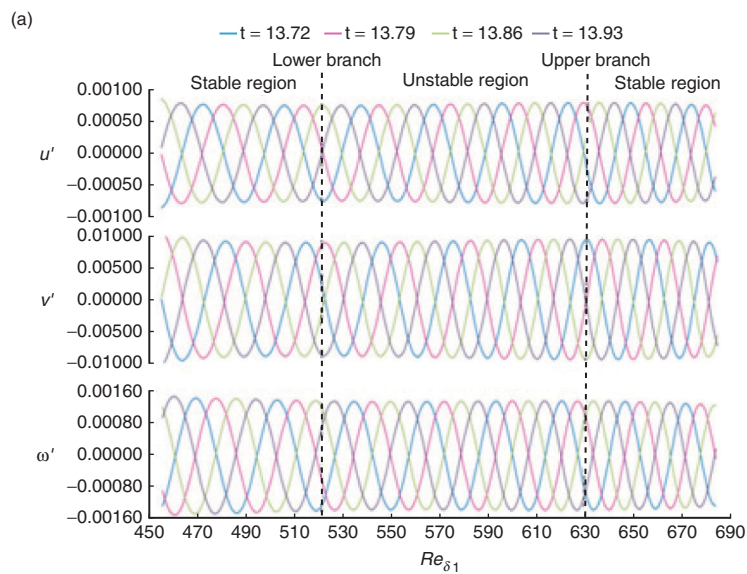


Figure 10. (Continued)

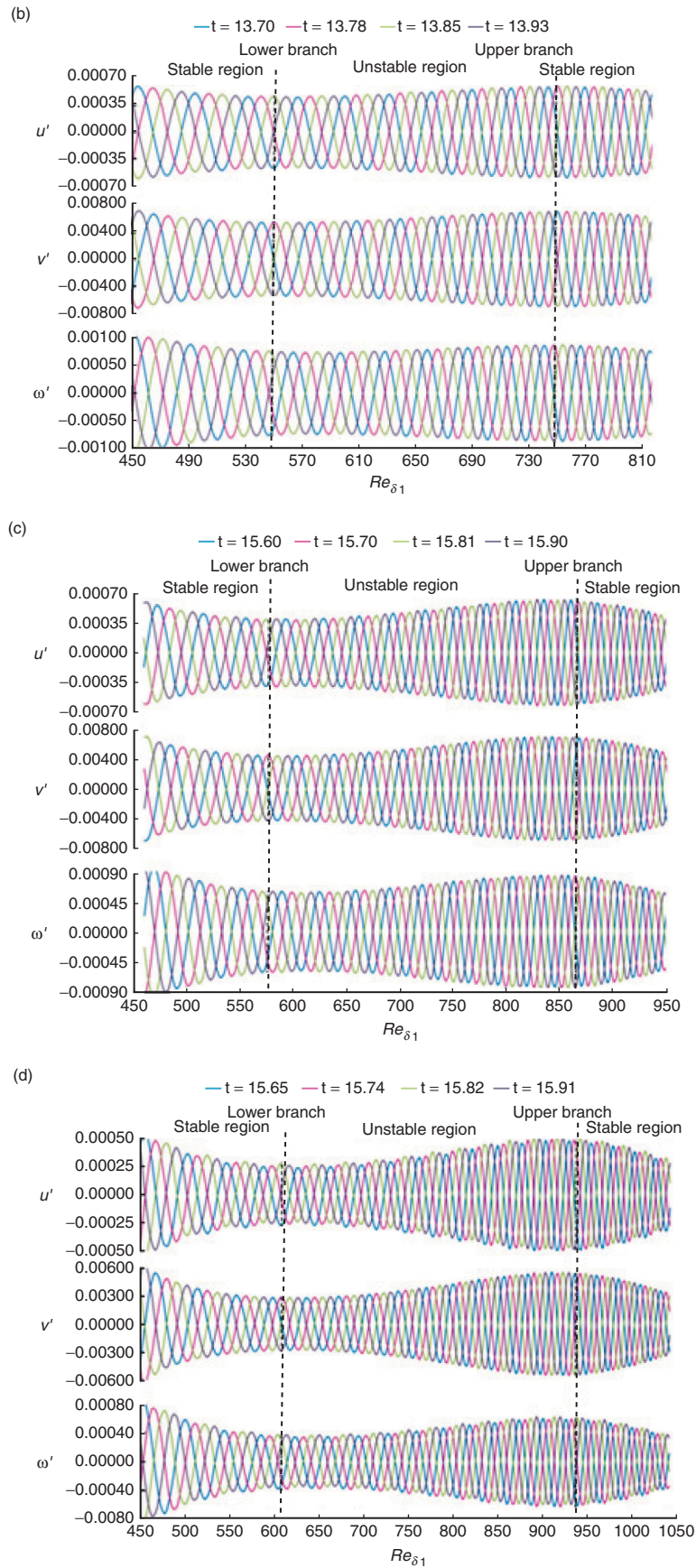


Figure 10. Wave amplification/damping for complete traverse of the neutral stability curve at four times and $y/\Delta y = 3$. Cases: (a) A, (b) B, (c) C, and (d) D.

patterns of damping in the stable region, amplification in the unstable region, and then damping again in the stable region. These patterns become more pronounced as the frequencies of the disturbances are reduced from Test Case A to D. Therefore, the results have shown that the wave interaction behavior is agreeable with linear stability theory when the flow conditions are in the linear stability regime.

5. CONCLUSION

I direct your attention to Figures 1a and 1b. This has been a deconstruction of the architecture of the classical problem of turbulence transition in boundary layer flow. Underneath the artifice of apparent cacophony of vexatious turbulent flow patterns lies a phenomenon that is governed by a symphony of laws in physics and mathematics. This study demonstrates a systematic approach to breaking down this complex problem by a progression of consideration of its multifarious aspects. Turbulence is an interweaving concept that encompasses interconnected interplay among its physical nature, mathematical representation, and numerical simulation.

For the physics, the objective is to understand the mechanisms that contribute to turbulence transition in boundary layer flows. The stages of turbulence development are observed to be receptivity, linear instability, non-linear instability, and breakdown to flow randomization. The physical processes up to the linear instability stage are well-understood and can be accurately described by linear stability theory and the OS equation. Beyond this stage, as the flow enters into the non-linear stages, the system behavior becomes shrouded in mystery. Some flow structures and patterns that have been consistently observed are the SCS structures, Λ -vortex, Ω -vortex, high shear layer, and harmonic wave generation. Their intricate interactions are not well understood. Among the challenges are the microscopic length scales of the flow structures and the infinitesimal magnitudes of the wave interactions. These obstacles have consistently confounded efforts to visualize turbulence transition behavior.

To attain a feasible solution to this problem requires first a conversion of the physical phenomenon into its corresponding mathematical representation. In the case of turbulent flow, the relevant mathematical equations are the NS equations along with the appropriate boundary conditions. For greater ease of problem definition and obtaining an accurate solution, the NS equations can be converted to the Vorticity Transport Equation. The conversion to the Vorticity Transport Equation leads to a concomitant set of equations that needs to be solved simultaneously. These equations are the continuity condition and the definition of vorticity. This set of equations is classically known as the Cauchy-Riemann type of equations or a div-curl pair of equations. The Cauchy-Riemann Equations have been extensively researched with many solution procedures possible. One popular method is to further break down the equations by taking a second curl of the definition of vorticity and combine the result with the continuity condition to produce a Poisson's Equation that is more amenable to numerical solutions. In taking the curl of the definition of vorticity, a derivative is taken of the vorticity. This operation generates a new problem in that the relation between the vorticity and the flow velocities is lost in the process. To recover this relationship, the definition of vorticity must be enforced at the boundaries as additional boundary conditions.

What remains in the mathematical representation are the boundary conditions. The boundary conditions for the inflow and wall are now generally accepted by the consensus of the fluid dynamics academic community. However, questions remain regarding the free stream and outflow boundary conditions, especially the latter. This is due to the fact that limitations in computational capacity in the present time preclude numerical simulations of systems of realistic physical dimensions. Rather, truncation of the computational domain is necessary at the free stream and outflow so that numerical computations will remain within practical limits. Truncation of the domain at these locations thus leads to artificial boundary conditions to be prescribed there that are not reflective of the physical situation but rather serve the need to maintain practical computational time. The free stream and outflow boundary conditions in this study are adopted from the classical work of Fasel, 1980 [44]. They have proven to be effective in generating valid numerical results of wave propagation in the boundary layer.

Turbulence transition contains microscopic-scale flow structures and infinitesimal amplitudes of wave interactions that have consistently confounded experimental methods of flow measurement and visualization. Thus, the need for numerical simulations. The mathematical representation of the Vorticity Transport equation and boundary conditions must be solved by a proper numerical method. Numerical simulations of the Vorticity Transport Equation meets with another problem, and that is, the

non-linearity of the equations renders them to be impractically time-consuming to be solved. To circumvent this problem, in this study, the Vorticity Transport Equation is solved by a linearized procedure with line iterations.

Numerical results of the two-dimensional case of wave propagation in the boundary layer are presented in this study. The flow conditions are in the linear instability region. The numerical results are then validated by comparison with results described by linear stability theory. Test cases of numerical experiments are run as adopted from the classical works of Fasel, 1980 [44]. Results show that the wave propagation behavior in the linear instability region does, in fact, agree with linear stability theory. In the stable region where wave interactions are expected to damp, damping is indeed observed. The same is true for the unstable region where wave interactions are conversely expected to amplify. Agreement with linear stability theory proves that the numerical model of this study is a valid approach that can then be extended into the investigation of the non-linear instability region leading to breakdown to flow randomization.

Fundamental understanding of turbulence transition intertwines interdisciplinary perspectives from physics, mathematics, and numerical computations. This has been an exercise in deconstructing this co-adjutant framework. Targeting the wave interactions in the linear instability region as the phenomena for visualization, converting the physical perspective into a well-posed, solvable mathematical representation, devising a numerical method that can robustly and efficiently solve the governing equations to generate realizations of the wave propagation behavior, then the fascinating problem of turbulence transition in boundary layer flow can be systematically broken down to gain full appreciation of its confounding complexity.

ACKNOWLEDGEMENTS

The authors are grateful for the support from Nanyang Technological University Grant RG 4/07 for this study. The authors are grateful to the publishers for granting the permission for reprinting.

REFERENCES

- [1] Kachanov, Y. S., Physical mechanisms of laminar-boundary-layer transition, *Annual Review of Fluid Mechanics*, 1994, 26, 411–482.
- [2] Schubauer, G. and Skramstad, H. K., Laminar boundary layer oscillations and stability of laminar flow, *Journal of Aeronautical Science*, 1947, 14, 69.
- [3] Herbert, T., Secondary instability of boundary layers, *Annual Review of Fluid Mechanics*, 1988, 20, 487–526.
- [4] Kachanov, Y. S. and Levchenko, V. Y., The resonant interaction of disturbances at laminar-turbulent transition in a boundary layer, *Journal of Fluid Mechanics*, 1984, 138, 209–247.
- [5] Zelman, M. B. and Maslennikova, I. I., Tollmien-Schlichting wave resonant mechanism for subharmonic-type transition, *Journal of Fluid Mechanics*, 1993, 252, 449–478.
- [6] Waleffe, F., The nature of triad interactions in homogeneous turbulence, *Physics of Fluids A*, 1992, 4(2), 350–363.
- [7] Orszag, S. A. and Patera, A. T., Secondary instability of wall-bounded shear flows, *Journal of Fluid Mechanics*, 1983, 128, 347–385.
- [8] Craik, A. D. D., Non-linear resonant instability in boundary layers, *Journal of Fluid Mechanics*, 1971, 50(2), 393–413.
- [9] Klebanoff, P. S., Tidstrom, K. D., and Sargent, L. M., The three-dimensional nature of boundary-layer instability, *Journal of Fluid Mechanics*, 1962, 12, 1–34.
- [10] Borodulin, V. I., Gaponenko, V. R., Kachanov, Y. S., Meyer, D. G. W., Rist, U., Lian, Q. X., and Lee, C. B., Late-stage transitional boundary-layer structures. Direct numerical simulation and experiment, *Theoretical and Computational Fluid Dynamics*, 2002 15, 317–337.
- [11] Gatski, T. B., Review of incompressible fluid flow computations using the vorticity-velocity formulation, *Applied Numerical Mathematics*, 1991, 7, 227–239.
- [12] Rempfer, D., On boundary conditions for incompressible Navier-Stokes problems, *Applied Mechanics Review*, 2006, 59, 107–125.
- [13] Gresho, P. M., Incompressible fluid dynamics: Some fundamental formulation issues, *Annual Review of Fluid Mechanics*, 1991, 23, 413–453.

- [14] Bhaganagar, K., Rempfer, D., and Lumley, J. L., Direct numerical simulation of spatial transition to turbulence using fourth-order vertical velocity second-order vertical vorticity formulation, *Journal of Computational Physics*, 2002, 180, 200–228.
- [15] Gatski, T. B., Grosch, C. E., and Rose, M. E., A numerical study of the two-dimensional Navier-Stokes equations in vorticity-velocity variables, *Journal of Computational Physics*, 1982, 48, 1–22.
- [16] Daube, O., Resolution of the 2D Navier-Stokes equations in velocity-vorticity form by means of an influence matrix technique, *Journal of Computational Physics*, 1992, 103, 402–414.
- [17] Ishihara, T., Gotoh, T., and Kaneda, Y., Study of high-Reynolds number isotropic turbulence by Direct Numerical Simulation, *Annual Review of Fluid Mechanics*, 2009, 41, 165–180.
- [18] Fasel, H., Investigation of the stability of boundary layers by a finite difference model of the Navier-Stokes equations, *Journal of Fluid Mechanics*, 1976, 78(2), 355–383.
- [19] Fasel, H. and Konzelmann, U., Non-parallel stability of a flat-plate boundary layer using the complete Navier-Stokes equations, *Journal of Fluid Mechanics*, 1990, 221, 311–347.
- [20] Fasel, H. F., Rist, U., and Konzelmann, U., Numerical investigation of the three-dimensional development in boundary-layer transition, *AIAA Journal*, 1990, 28(1), 29–37.
- [21] Gatski, T. B., Grosch, C. E., and Rose, M. E., The numerical solution of the Navier-Stokes equations for 3-dimensional, unsteady, incompressible flows by compact schemes, *Journal of Computational Physics*, 1989, 82, 298–329.
- [22] Rai, M. M. and Moin, P., Direct numerical simulation of transition and turbulence in a spatially evolving boundary layer, *Journal of Computational Physics*, 1993, 109(2), 169–192.
- [23] Kleiser, L. and Zang, T. A., Numerical simulation of transition in wall-bounded shear flows, *Annual Review of Fluid Mechanics*, 1991, 23, 495–537.
- [24] Barry, M. D. J. and Ross, M. A. S., The flat plate boundary layer. Part 2. The effect of increasing thickness on stability, *Journal of Fluid Mechanics*, 1970, 43(4), 813–818.
- [25] Jordinson, R., The flat plate boundary layer. Part 1. Numerical integration of the Orr-Sommerfeld equation, *Journal of Fluid Mechanics*, 1970, 43(4), 801–811.
- [26] Ross, J. A., Barnes, F. H., Burns, J. G., and Ross, M. A. S., The flat plate boundary layer. Part 3. Comparison of theory with experiment, *Journal of Fluid Mechanics*, 1970, 43(4), 819–832.
- [27] Laney, C. B., *Computational Gasdynamics*, Cambridge University Press, Cambridge, 1998.
- [28] Chung, T. J., *Computational Fluid Dynamics*, Cambridge University Press, Cambridge, 2002.
- [29] Lee, C. B. and Wu, J. Z., Transition in wall-bounded flows, *Applied Mechanics Review*, 2008, 61, 1–20.
- [30] Sengupta, T. K., Bhaumik, S., Singh, V., and Shuki, S., Nonlinear and nonparallel receptivity of zero-pressure gradient boundary layer, *International Journal of Emerging Multidisciplinary Fluid Sciences*, 2009, 1(1), 19–35.
- [31] Ng, B. S. and Reid, W. H., On the numerical solution of the Orr-Sommerfeld problem: Asymptotic initial conditions for shooting methods, *Journal of Computational Physics*, 1980, 38, 275–293.
- [32] Van Stijn, T. L. and Van de Vooren, A. I., An accurate method for solving Orr-Sommerfeld equation, *Journal of Engineering Mathematics*, 1980, 14(1), 17–26.
- [33] Orszag, S. A., Accurate solution of the Orr-Sommerfeld stability equation, *Journal of Fluid Mechanics*, 1971, 50, 689–703.
- [34] Bertolotti, F. P., Herbert, T., and Spalart, P. R., Linear and nonlinear stability of the Blasius boundary layer, *Journal of Fluid Mechanics*, 1992, 242, 441–474.
- [35] Benney, D. J. and Lin, C. C., On the secondary motion induced by oscillations in a shear flow, *Physics of Fluids*, 1960, 3(4), 656–657.
- [36] Bake, S., Fernholz, H. H., and Kachanov, Y. S., Resemblance of K- and N-regimes of boundary layer transition at late stages, *European Journal of Mechanics B - Fluids*, 2000, 19, 1–22.
- [37] Bake, S., Meyer, D. G. W., and Rist, U., Turbulence mechanism in Klebanoff transition: A quantitative comparison of experiment and direct numerical simulation, *Journal of Fluid Mechanics*, 2002, 459, 217–243.

- [38] Champagne, F. H., Harris, V. G., and Corrsin, S., Experiments on nearly homogeneous turbulent shear flow, *Journal of Fluid Mechanics*, 1970, 41(1), 81–139.
- [39] E, W. and Liu, J.-G., Vorticity boundary condition and related issues for finite difference schemes, *Journal of Computational Physics*, 1996, 124, 368–382.
- [40] Orszag, S. A. and Israeli, M., Numerical simulation of viscous incompressible flows, *Annual Review of Fluid Mechanics*, 1974, 6, 281–318.
- [41] Wu, X. H., Wu, J. Z., and Wu, J. M., Effective vorticity-velocity formulations for three-dimensional incompressible viscous flows, *Journal of Computational Physics*, 1995, 122, 68–82.
- [42] Davies, C. and Carpenter, P. W., A novel velocity-vorticity formulation of the Navier-Stokes equations with applications to boundary layer disturbance evolution, *Journal of Computational Physics*, 2001, 172, 119–165.
- [43] Bertagnolio, F. and Daube, O., Solution of the div-curl problem in generalized curvilinear coordinates, *Journal of Computational Physics*, 1997, 138, 121–152.
- [44] Fasel, H., ed. *Recent Developments in the Numerical Solution of the Navier-Stokes Equations and Hydrodynamic Stability Problems*, Computational Fluid Dynamics, ed. Wolfgang Kollmann, 1980, Hemisphere Publishing Corporation, 167–280.